Multipoint detection of structural deformation of pulsating 3D heart model using flexible organic piezoelectric-sensor array

Nagayama, Yusaku ; Kondo, Yuya ; Koshiba, Yasuko ; Horike, Shohei ; Takashima, Kazuto ; Ishida, Kenji

(Citation)
Japanese Journal of Applied Physics,61(SE):SE1014

(Issue Date)
2022-06-01

(Resource Type)
journal article

(Version)
Version of Record

(URL)
https://hdl.handle.net/20.500.14094/90009252

REGULAR PAPER • OPEN ACCESS

Multipoint detection of structural deformation of pulsating 3D heart model using flexible organic piezoelectric-sensor array

To cite this article: Yusaku Nagayama *et al* 2022 *Jpn. J. Appl. Phys.* **61** SE1014

OPEN ACCESS

Japanese Journal of Applied Physics **61**, SE1014 (2022) **REGULAR PAPER**

https://doi.org/10.35848/1347-4065/ac5a04

Multipoint detection of structural deformation of pulsating 3D heart model using flexible organic piezoelectric-sensor array

Yusaku Nagayama[1], Yuya Kondo[1], Yasuko Koshiba[1,2], Shohei Horike[1,2,3], Kazuto Takashima[4], and Kenji Ishida[1,2*]

[1]*Department of Chemical Science and Engineering, Graduate School of Engineering, Kobe University, 1-1 Rokkodai-cho, Nada-ku, Kobe 657-8501, Japan*

[2]*Research Center for Membrane and Film Technology, Kobe University, 1-1 Rokkodai-cho, Nada-ku, Kobe 657-8501, Japan*

[3]*PRESTO, Japan Science and Technology Agency, Kawaguchi 332-0012, Japan*

[4]*Graduate School of Life Science and Systems Engineering, Kyushu Institute of Technology, 2-4 Hibikino, Wakamatsu-ku, Kitakyushu 808-0196, Japan*

*E-mail: kishida@crystal.kobe-u.ac.jp

Received November 15, 2021; revised January 31, 2022; accepted March 2, 2022; published online April 5, 2022

Multipoint detection of the structural deformation of a pulsating 3D heart model was conducted using a flexible piezoelectric sensor array with a poly(vinylidene fluoride-trifluoroethylene) [P(VDF-TrFE)] thin film sealed with biocompatible parylene C. The piezoelectric signals detected from the sensor array attached to the 3D heart model were correlated with an electrocardiogram signal. These piezoelectric signals can be converted into the compressive stress applied to the flexible sensors by the pulsating motion of the 3D heart model. The experimental results mean that the contraction force, generated by the heart muscle (i.e., myocardium), can be directly evaluated. The different output voltages depending on the location were obtained from each sensor, indicating the possibility of a real-time detection of the irregular motion of the heart and the early detection of ischemic heart disease, which leads to the loss of local contractile force in myocardial tissue.

1. Introduction

In recent years, significant progress has been made in the research and development of new medical devices that can acquire information on pathological conditions and automatically administer drugs using medical sensors fixed in the body.[1–3] These devices are called "implantable" devices and are attracting attention as the next generation of medical engineering technology to support patient recovery, disease management, and quality of life (QOL).[4–8] For example, a pacemaker is one of the typical implantable medical devices; it sends electrical signals to the heart to set the proper pace of the heartbeat.[9,10] Today, millions of people have been implanted with pacemakers to control their heartbeat in real time for supporting their healthy life.

The human heart is a powerful muscle, pumping blood to ensure that all the organs in the body receive sufficient oxygen and nutrients to function appropriately, and is a vital organ that is necessary for survival. Through the regular contraction and expansion of the heart muscle, blood is pumped out of the heart to all the organs in the body. This movement of the heart muscle (contraction and dilation) is observed as a heartbeat. Unlike the arm and leg muscles, the contraction of the heart muscle is involuntary, that is, the timing of its contraction or dilation cannot be varied at will. Therefore, monitoring the abnormalities in the heartbeat is important for the early detection of heart diseases.

Heartbeat (motion of myocardium) is caused by the electrical signals generated by the medulla oblongata. Electrocardiograms (ECGs) have been widely used to detect heart diseases; however, in principle, the ECG does not observe the motion of myocardium on the beating heart, but only detects these electrical signals through a transmitter system; therefore, specific heart diseases caused by disorders in the heart muscle (such as pericarditis, myocardium weakness, and necrosis caused by blood-vessel blockage) can be barely detected using ECG until the disease becomes serious.[11–14] In contrast, the use of implantable devices that can directly detect myocardial beats is an innovative method to detect the abnormalities and tissue changes in the heart muscle, which may be unknown to a person, such as myocardial infarction and cardiomyopathy in its early stages. However, only a few studies have reported the direct detection of myocardial motion.

The use of self-powered implantable devices based on lead zirconate titanate (PZT) has been reported.[15–18] PZT, a typical inorganic piezoelectric material with a large piezoelectric coefficient, acts as a heart-rate sensor and piezoelectric power generator in vivo; however, it contains toxic lead, which poses a significant medical obstacle to its implantation in living tissue. In addition, PZT is often a ceramic, resulting in several disadvantages, such as brittle fracture owing to deformation and its interference with the movement and functioning of muscles and organs. Therefore, the use of organic piezoelectric materials is preferrable for in vivo devices. Considering the softness and slow movement of organs in vivo, organic piezoelectric materials with excellent flexibility, stability, and biocompatibility are suitable for implantable movement sensors of the heart.

In our previous study, we reported on the heart-rate detection and power generation from heartbeats using flexible organic piezoelectric devices and a pulsating 3D heart model.[19] These devices were fabricated using an organic ferroelectric polymer, poly(vinylidene fluoride/trifluoroethylene) [P(VDF-TrFE)], which has been widely studied for its ferroelectricity, piezoelectricity, and pyroelectricity.[20–26] We demonstrated the potential of this single-sensor device to simultaneously perform vital sensing and electric power generation.

However, the heartbeat is caused by a complex motion of the myocardial tissue; therefore, the deformation intensity and timing differ according to the local part of the heart. To detect such complex motions in detail with a high position resolution, it is insufficient to use a single- sensor alone. In this context, 2D monitoring of heartbeats (i.e., mapping of stretching stress caused by the deformation on the heart) via the multiple-point sensing may be useful in identifying the sites of abnormalities in the heart before the diseases become serious. But a few studies have reported on multipoint detection using implantable piezoelectric devices.

In this study, the flexible P(VDF-TrFE) sensor array with nine sensors, sealed with biocompatible layer,[27] was fabricated, and the structural and piezoelectric properties were evaluated. The time variation of the structural deformation of the pulsating 3D heart model during the heartbeat was investigated by the multipoint detection using the flexible piezoelectric P(VDF-TrFE) sensor arrays.

2. Experimental methods

P(VDF-TrFE) [Fig. 1(a)] consisting of a 75/25 VDF-TrFE molar content ratio (Sigma-Aldrich Solvene250/P300) was dissolved in 7 wt% methyl ethyl ketone (MEK). The solution was spin-coated onto a Al coated 25 μm thick PEN films. The P(VDF-TrFE) films were annealed at 130 °C for 1.5 h to convert P(VDF-TrFE) from a paraelectric Form II crystal to ferroelectric Form I crystal. Then, Al was vacuum-deposited as the top electrode. The single piezoelectric sensor structure of Al/P(VDF-TrFE) (1 μm)/Al was fabricated with a sensor area of 1.0 mm × 1.0 mm. A sensor array with nine sensors was fabricated on an area of 10.0 mm × 10.0 mm in the same way.

A poly(monochloro-paraxylene) (parylene C), serving as a biocompatible layer as shown in Fig. 1(b), was coated on the P(VDF-TrFE) film by vapor deposition polymerization using a laboratory-made chamber. Not only the top of the device, but the entire surface of devices was then sealed with 1 μm thick parylene C [Fig. 1(c)].

These films were evaluated by Fourier transform infrared (FT-IR) spectroscopy using the JASCO FT/IR-660Plus spectrometer. The process of electrical poling and evaluating the electrical displacement versus electrical field (*D*–*E* hysteresis) was performed by applying a triangular electric field using a ferroelectric measurement system (TOYO Corporation Model 6252 Rev. C). The flexible P(VDF-TrFE) sensor arrays were attached to a 3D heart model (cross Medical 3D heart pulsation model coronary bypass training system XC-01TP regular adult pulsating model), that simulated a beating heart. The output voltage from the sensor was measured using an operational amplifier and oscilloscope.

3. Results and discussion

3.1. Evaluation of P(VDF-TrFE) films sealed with parylene C

Figure 2(a) shows the FT-IR spectra of the parylene C, P(VDF-TrFE), and P(VDF-TrFE)/parylene C stacked films prepared on Si substrates. In the spectrum of the P(VDF-TrFE) film, the absorption peaks were observed at 1295, 1195, 1078, and 850 cm^{-1}, corresponding to the ferroelectric crystal phase Form I of P(VDF-TrFE).[28,29]

In contrast, in the spectrum of the parylene C film, the absorption peaks related to aromatic C–C stretching vibration at 1495 cm^{-1}, CH_2 rocking vibration at 1452 cm^{-1}, Cl bonded to aromatic ring vibration at 1051 and 877 cm^{-1}, and out-of-plane C-H wagging vibration at 820 cm^{-1} could all be assigned to parylene C.[30,31] In the P(VDF-TrFE)/parylene C-stacked film spectrum, the absorption peaks related to the ferroelectric crystal phase Form I of P(VDF-TrFE) and parylene C were observed. VDF-based materials typically have three crystal phases,[32] and phases I and III exhibit ferroelectricity. The P(VDF-TrFE) thin film that was prepared as ferroelectric Form I did not change even after the parylene C deposition process.

Figure 2(b) shows the *J*–*E* switching and *D*–*E* hysteresis curves of the P(VDF-TrFE)/parylene C stacked film. Clear current peaks corresponding to polarization switching and *D*–*E* hysteresis loops can be observed. These results indicate that the P(VDF-TrFE) thin films sealed with parylene C exhibit ferroelectricity and are expected to exhibit piezoelectricity as well.

3.2. Detection of heart rate using single-sensor device

Before multipoint detection using sensor arrays, piezoelectric-response measurements were performed using a single-

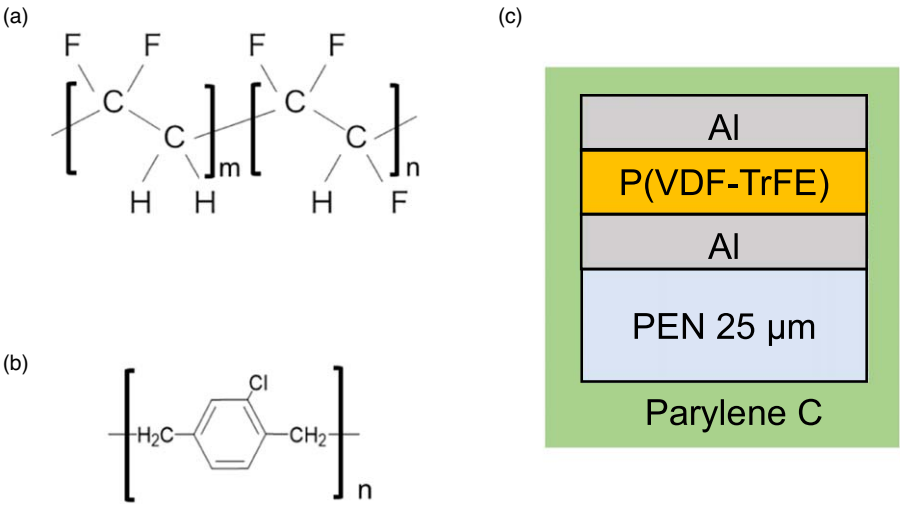

Fig. 1. (Color online) Molecular structure of (a) P(VDF-TrFE) and (b) parylene C, and (c) schematic structure of flexible piezoelectric devices.

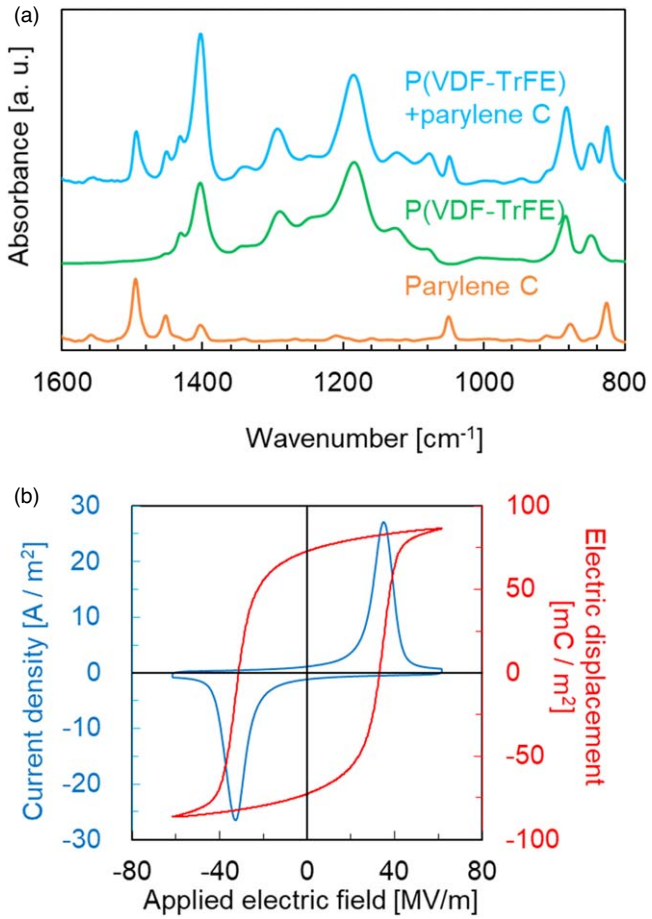

Fig. 2. (Color online) (a) FT-IR spectra of the P(VDF-TrFE), parylene C, and P(VDF-TrFE)/parylene C stacked films. (b) *J*–*E* and *D*–*E* curves of the piezoelectric device sealed with parylene C.

sensor device. Figures 3(a) and 1(c) show a photograph and the structure of the flexible piezoelectric device, respectively. After poling, the flexible piezoelectric sensors were attached to the right ventricle (RV) of the 3D heart model [Fig. 3(b)]. The flexible sensors could follow the curved shape of the 3D heart model because of its flexibility. Figure 3(c) shows the circuit diagram of the output voltage-measurement system. The output voltage was monitored using an oscilloscope, and an operational amplifier was used as the *I*–*V* converter.

Figure 3(d) shows the typical output voltage waveform obtained using the 3D heart model at a heart rate of 60 beats per minute (bpm). With the beating of the 3D heart model, the piezoelectric response corresponding to its pulsation was obtained. A negative output voltage was observed during the contraction of the 3D heat model, and a positive output voltage was observed during the expansion. These negative and positive output-voltage cycles were repeated according to a 1 s cardiac cycle.

Furthermore, the waveform has four main peaks per cycle; two peaks on the negative side (peaks A and B) and two peaks on the positive side (peaks C and D). In Fig. 3(d), t_1 corresponds to the time difference between the RV and LV contractions, and t_2 corresponds to the time difference between the RV and LV expansions of the 3D heart model. To reproduce the heart motion of healthy adults under normal conditions, for the heart rate of 60 bpm, t_1 and t_2 were set to 0.205 s and 0.225 s, respectively. Therefore, peaks A and C were observed with respect to the movement of the RV, and peaks B and D were derived from the movement of the LV, as shown in Fig. 3(e). The single-sensor sealed with parylene C could detect the pulsation of the 3D heart model accurately. The value of the output voltage was comparable to that of the unsealed devices. These results indicate that the sealing treatment with parylene C does not affect the detection of piezoelectric devices.

Figure 4 (a) shows the outline of the waveform of an electrocardiogram (ECG)[14] and the output voltage waveform obtained from the flexible piezoelectric sensor. The ECG waveform consists of P, QRS, and T waves. The P wave is observed to be due to the atrial depolarization caused by electrical signals from the sinoatrial node, resulting in the contraction of the left and right atria. The QRS wave caused by ventricular depolarization relates to the contraction of the LV and RV, and the T wave due to ventricular repolarization relates to the relaxation of the LV and RV. In contrast, in the flexible piezoelectric sensor, a negative output voltage is observed during contraction and a positive output voltage is observed during expansion. While the ECG uses electrodes placed on the surface of the body to detect the sum of the electrical activity that causes the heart to beat, the flexible piezoelectric sensor attached to the heart surface can directly evaluate the complex motion of the heart model, such as the deformation direction and magnitude on the pulsating. Despite the differences between the two measurement principles, there was an important correlation between the two waveforms to understand the condition of the heart.

Here, in order to estimate the force generated by the heart muscles, we attempted to analyze the local stress applied to the piezoelectric film from the obtained electrical signals. The piezoelectric current (I) of the uniaxial stretched polymer films is expressed as follows;

$$I = A\left(d_{31}\frac{d\sigma_1}{dt} + d_{32}\frac{d\sigma_2}{dt} + d_{33}\frac{d\sigma_3}{dt}\right), \quad (1)$$

where A is the electrode area, d_{31}, d_{32}, and d_{33} is the piezoelectric constant for the materials, and t is the time. σ_1 is the applied stress in the stretched direction (generally, the direction of long-chain axis), σ_2 is the applied stress in the transverse direction, and σ_3 is the perpendicularly applied stress to the film surface. When the flexible piezoelectric films are shrinking and/or stretching with the pulsating motion of the 3D heart model, the piezoelectric current was generated by the combination of d_{31}, d_{32}, and d_{33}. However, it is well-known that the output current from the piezoelectric thin film in the lateral direction is much higher than that in the vertical direction,[33] dominating the effect of d_{33} by d_{31} for the output current during the film bending. Assuming that the piezoelectric effect is isotropic in in-plane direction of the unstretched P(VDF/TrFE) film ($d_{31} = d_{32}$). Equation (1) can be simplified under a spherical shell model such as the 3D heart model as follows;

$$I = 2A\, d_{31}\frac{d\sigma_1}{dt}. \quad (2)$$

The current has been converted to the voltage with the transimpedance gain of 10^7 V A^{-1} used in this study. Then, integrating Eq. (2) with respect to time yields the following equation:

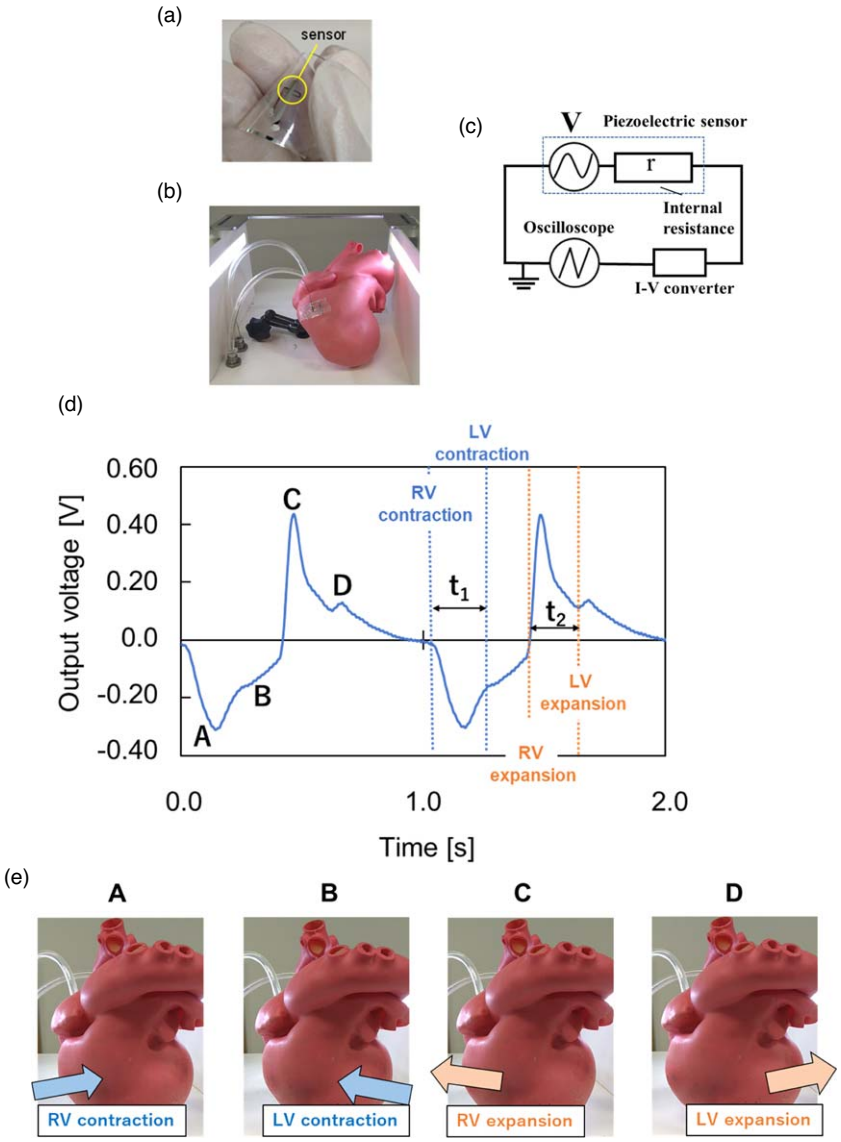

Fig. 3. (Color online) Photographs of the (a) flexible piezoelectric sensor and (b) sensor attached to the 3D heart model, (c) circuit diagram of the heartbeat-measurement system, (d) output-voltage curve detected on the RV at 60 bpm, and (e) photographs of 3D heart model showing contraction and expansion of LV and RV.

$$\sigma = \frac{\int V dt}{2Ad_{31} \times 10^7}. \quad (3)$$

We used $d_{31} = 10.7\ \mathrm{pm\ V^{-1}}$ as the piezoelectric constant.[34] Consequently, the output voltage can be converted into the stress applied to the flexible sensors during the heart-model operation. Figure 4(b) shows the time-variation of the output voltage and the corresponding stress estimated using Eq. (3), which can directly detect the stress during pulsating the 3D heart model.

At $t = 0$ s [stage (i) in Fig. 4(b)], the heart model is maximally inflated to simulate the diastole period in the cardiac cycle. In this study, we define the stress as zero ($\sigma = 0$) on this inflated condition. From $t = 0$ to 0.5 s [stage (ii) in Fig. 4(b)], the 3D heart model contracted, simulating the systole period. Since the flexible sensor undergoes compressive stress during the shrinking motion of the heart model, the piezoelectric voltage shows a negative value. After $t = 0.5$ s, the 3D heart model starts to expand. As the direction of deformation reverses due to the expansion of the heart, the piezoelectric voltage reverses to a positive value. By the expansion of the heart model, the compressive stress decreases and returns to the initial value at stage (iii) of Fig. 4(b).

This type of direct monitoring of the heartbeat cannot be performed using conventional ECGs. Furthermore, the points with abnormalities in the heart can be identified by mapping the stress via multiple sensors.

3.3. Pulsation detection using piezoelectric-sensor array

The sensor array was fabricated for multipoint detection of the pulsation deformation. Nine sensors were placed on the device with an area of 10.0 mm × 10.0 mm and each sensor was numbered from 1 to 9, as shown in Fig. 5(a). The P_r value of all the sensors was adjusted to 60 mC $\mathrm{m^{-2}}$ to ensure the same performance of each piezoelectric sensor. Subsequently, the sensor array was attached to the RV of the 3D heart model, and the output voltage from each sensor was measured.

Figure 5(b) depicts the output-voltage curves obtained from the sensor array attached to the 3D heart model at a

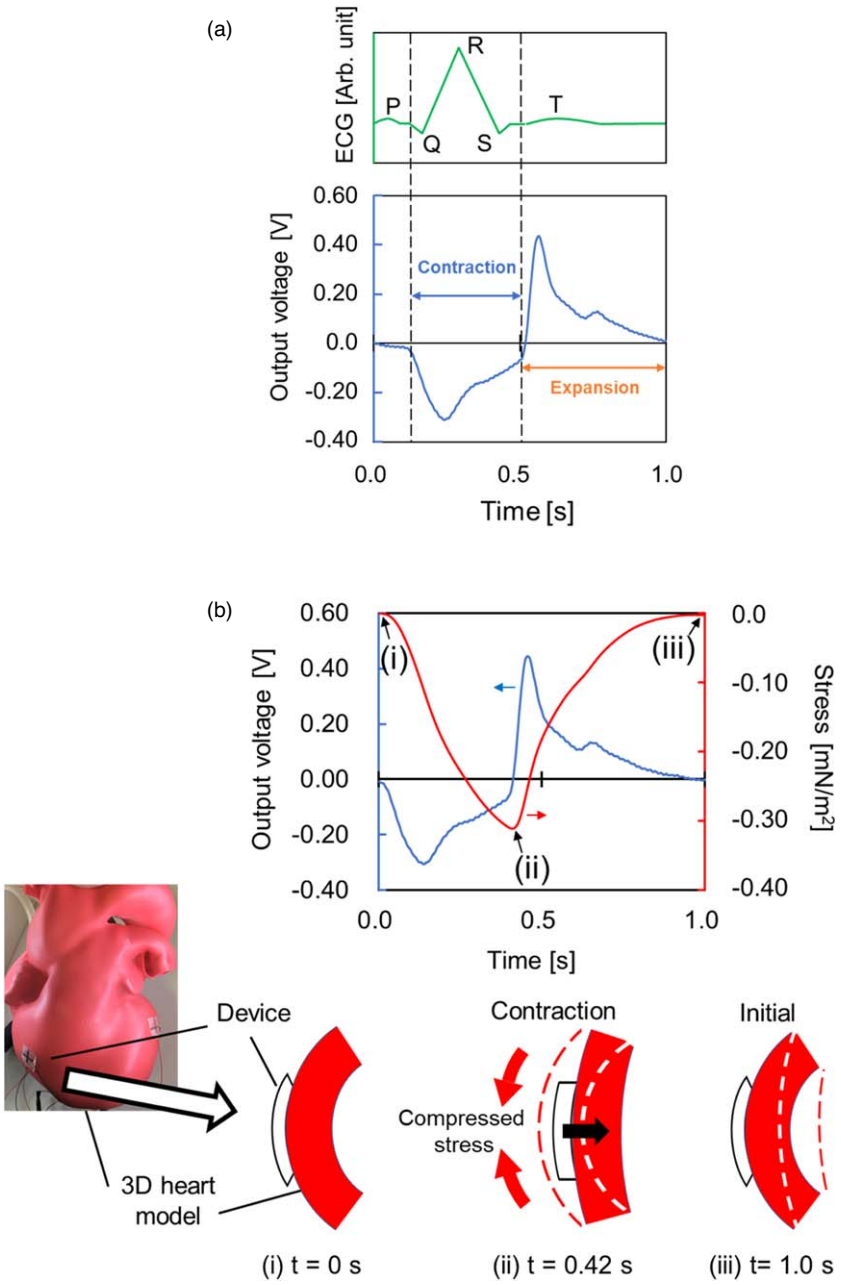

Fig. 4. (Color online) (a) Comparison of the outline of a typical ECG curve (green line) and the output-voltage waveform detected by the piezoelectric sensor (blue line). (b) Output-voltage curve and time variation of stress obtained from the output voltage.

heart rate of 60 bpm. The output voltage was negative during contraction and positive during expansion, being similar to that of the single-sensor device as shown in Fig. 3(d). The insets of Fig. 5(b) show enlarged views of the output-voltage curves. According to the location of each sensor, the value of the peak voltages, as well as the characteristic times corresponding to the maximum peak voltages, differed. The time variations of the peak voltages suggest that the pulsating heart model has complex deformation, where local deformations are transmitted on the heart model surface with time.

To highlight this potential capability of multipoint sensing, we demonstrated the mapping of the time and maximum value of the voltage peak. Figures 6(a) and 6(b) show the mapping of the time "T" when the observed piezoelectric voltage reaches its maximum value, during the expansion and contraction of the heart model, respectively. Considering that the observation area is maximally deformed at time "T", the expanding motion [Fig. 6(a)] in the vicinity of sensor 1 occurs earlier than that of sensor 6, whereas the contracting motion provides faster responses to sensors 1 and 2 than those to sensors 5 and 8.

In contrast, the peak-top voltage provides information on the position-dependent deformation intensity of the heart model. Figure 7 shows the output voltage from the sensor array under the 4 characteristic time periods of the cardiac cycle (t_A: RV contraction, t_B: LV contraction, t_C: RV expansion, t_D: LV expansion), as shown in Fig. 5(b). As mentioned above, the output-voltage values from the sensors represent the local stress applied to the piezoelectric sensor due to the pulsating of the 3D heart model. Comparing the RV motion (t_B and t_D) with the LV motion (t_A and t_C), the difference in the output voltages between the sensors is found to be smaller for the LV. When the LV is deformed, its movement propagates through the heart surface to the RV,

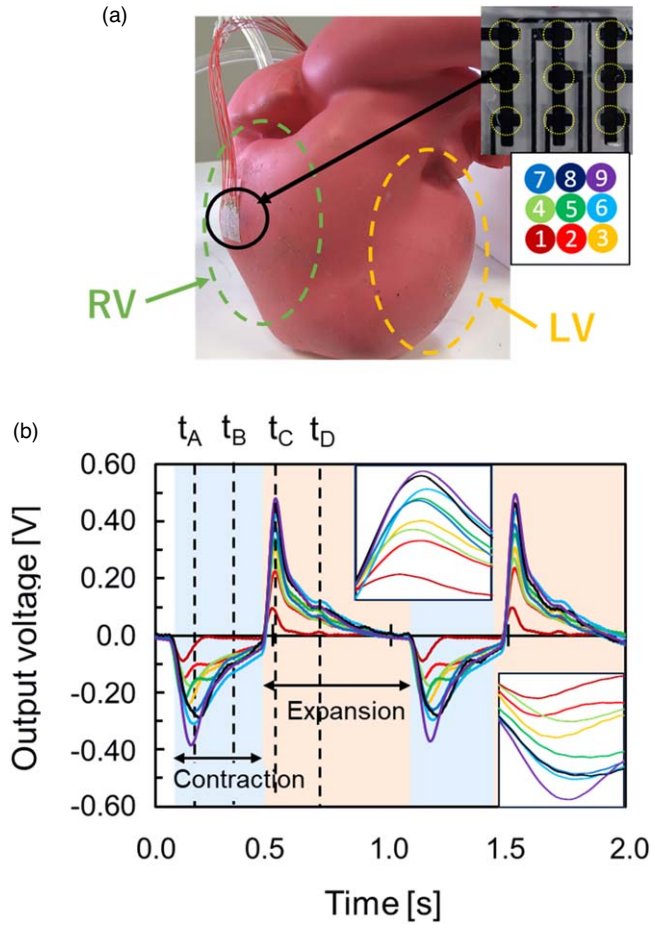

Fig. 5. (Color online) (a) Photograph of the 3D heart model and sensor array (inset), and the number and color (inset) of the nine sensors, and (b) output-voltage curves obtained from each sensor. The color of the curves corresponds to the color shown in the inset of (a).

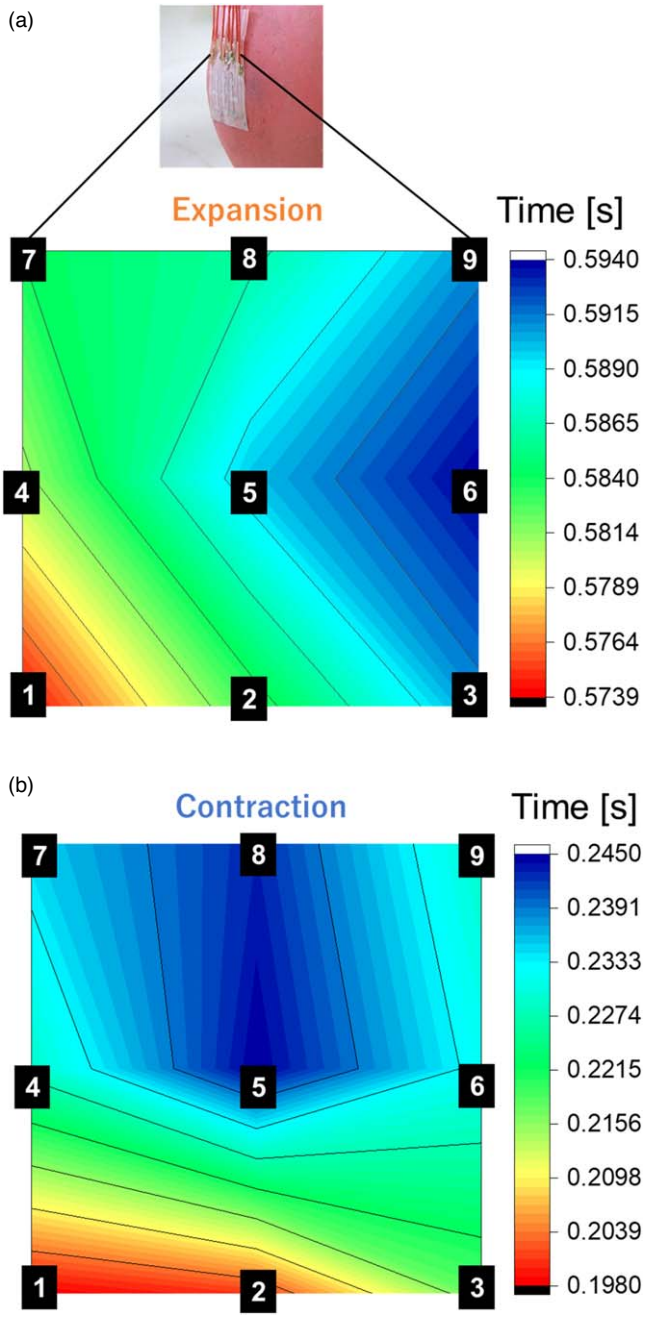

Fig. 6. (Color online) Time maps corresponding to the maximum-output voltage during (a) expansion and (b) contraction.

and the RV becomes stressed. In this experiment, the sensor array was attached to the RV; therefore, it was assumed that the deformation due to the LV movement was less dependent on the RV movement.

Comparing the output voltage values from each sensor, the value from sensor 9 was found to be the largest and that from sensor 1 was the smallest. Hence, it could be deduced that the displacement was large near sensor 9 and small near sensor 1 during both contraction and expansion of the RV. As such, the difference in displacement within an area of 10.0 mm × 10.0 mm can be detected at 3.5 mm intervals using the piezoelectric sensor array. This type of monitoring of time variations of voltages as well as their intensities during the complex deformation process of the heartbeat with a high position resolution can be only achieved using multipoint sensor arrays, which enable users to detect the early stages of cardiac diseases (e.g., pericarditis) via sensory data corresponding to slight abnormal deformations (both intensity and timing) of the heart.

4. Conclusions

In this study, we investigated the multipoint detection of the deformation of a 3D heart model using a flexible piezoelectric-sensor array. First, we evaluated the characteristics of P(VDF-TrFE) thin films sealed with parylene C, which is a common sealant for implantable devices owing to its biocompatibility. From the FT-IR spectra and the *D*–*E* and *J*–*E* curves, it was observed that the structure and ferroelectric properties of the P(VDF-TrFE) thin films were not affected by the parylene C sealing. The piezoelectric sensors were attached to a 3D heart model; the sensors followed the curved shape of the model owing to their flexibility. The output-voltage waveform was obtained from the piezoelectric sensor in accordance with the pulsation of the 3D heart model.

The waveform of the output voltage could be related to the waveform of the ECG; therefore, we believe that the proposed piezoelectric sensor has the potential to be used in the detection of heartbeats. In contrast, we could convert the output voltage into the stress applied to the piezoelectric sensors during the heart-model operation for both expansion and contraction, which is one of the advantages of direct

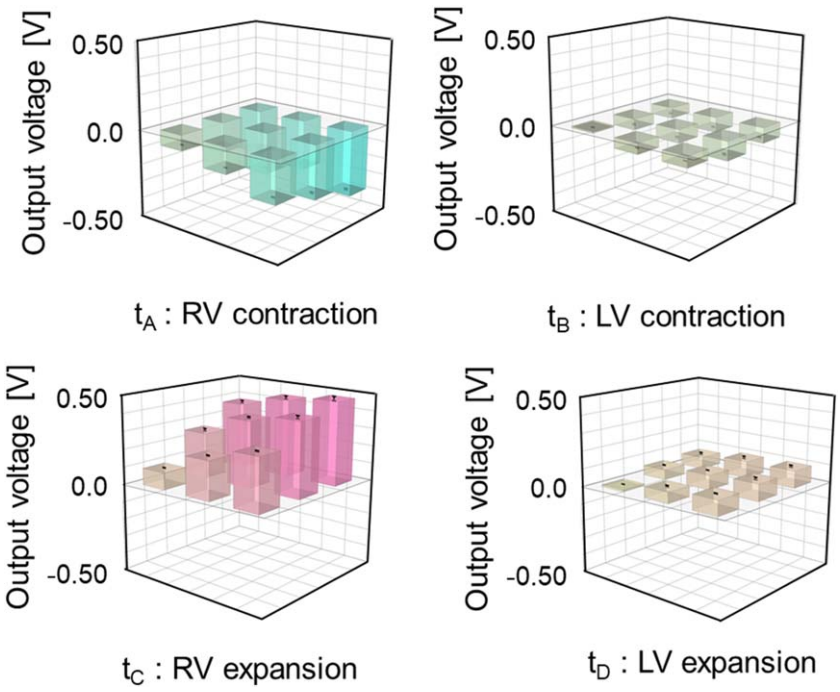

Fig. 7. (Color online) Output-voltage mapping of nine sensors at t_A (RV contraction), t_B (LV contraction), t_C (RV expansion), and t_D (RV expansion).

motion sensing using piezoelectricity over the conventional ECG. For multipoint detection, different output-voltage values were obtained at different locations on the 3D heart model at a 3.5 mm interval spacing during the beating of the heart. Mapping the output voltage and the time of the voltage peaks during the heartbeat using multipoint sensors indicated that the intensity and timing of heart motion differ according to the position of the heart, even in a small area (1 cm^2). Such a direct and precise monitoring of the complex heart deformation is expected to provide useful information on the early detection of cardiac diseases.

Acknowledgments

This work was partly supported by CREST and JSPS KAKENHI. S.H. would like to thank JST PRESTO.

ORCID iDs

Yasuko Koshiba https://orcid.org/0000-0001-7189-0109
Shohei Horike https://orcid.org/0000-0002-9656-0103
Kazuto Takashima https://orcid.org/0000-0002-3304-4443
Kenji Ishida https://orcid.org/0000-0003-1227-9638

1) T. Sekine, D. Kumaki, and S. Tokito, J. Soc. Photography Imaging Jpn. **82**, 10 (2019).
2) J. M. Maloney, S. A. Uhland, B. F. Norman, F. Sheppard Jr., C. M. Pelta, and J. T. Santini Jr., J. Control. Release **109**, 244 (2005).
3) I. Mendez et al., Nat. Med. **5**, 14 (2008).
4) D. H. Keum et al., Sci. Adv. **6**, 3252 (2020).
5) J. Viventi et al., Neuroscience. **12**, 14 (2011).
6) T. Sekitani et al., Nat. Commun. **7**, 11425 (2016).
7) B. Gil, B. Li, A. Gao, and G. Z. Yang, ACS Appl. Electron. Mater. **2**, 2669 (2020).
8) Z. Xu et al., Healthcare Mater. **10**, 2002100 (2021).
9) D. Birnie, K. Williams, A. Guo, L. Mielniczuk, D. Davis, R. Lemery, M. Green, M. Gollob, and A. Tang, Am. J. Cardiol. **98**, 93 (2006).
10) V. M. Christoffels, G. J. Smith, A. Kispert, and A. F. M. Moorman, Circ. Res. **106**, 240 (2010).
11) M. Imazio and F. Gaita, Heart **14**, 101 (2015).
12) R. W. Troughton, C. R. Asher, and A. L. Klein, Lancet **363**, 9410 (2004).
13) R. B. Singh, D. Pella, N. S. Neki, J. P. Chandel, S. Rastogi, H. Mori, K. Otsuka, and P. Gupta, Biomed. Pharmacother. **58**, 116 (2004).
14) Y. Wang, F. Agrafioti, D. Hatzinakos, and K. N. Plataniotis, EURASIP J. Adv. Signal Process. **2008**, 148658 (2007).
15) B. İlik, A. Koyuncuoğlu, Ö. Ş. Sukas, and H. Külah, Sens. Actuators **280**, 38 (2018).
16) M. G. Kang, W. S. Jung, C. Y. Kang, and S. J. Yoon, Actuators **5**, 5010005 (2016).
17) K. Park et al., Adv. Mater. **26**, 2514 (2014).
18) C. Dagdeviren et al., Proc. Natl Acad. Sci. U.S.A. **111**, 1927 (2014).
19) Y. Kondo, S. Horike, Y. Koshiba, T. Fukushima, and K. Ishida, Jpn. J. Appl. Phys. **59**, SDDF02 (2020).
20) H. Kawai, J. Appl. Phys. **8**, 975 (1969).
21) M. Fukagawa, Y. Koshiba, T. Fukushima, M. Morimoto, and K. Ishida, Jpn. J. Appl. Phys. **57**, 04FL06 (2018).
22) A. Kobayashi, Y. Koshiba, Y. Ueno, T. Kajihara, Y. Tsujiura, M. Morimoto, S. Horike, T. Fukushima, I. Kanno, and K. Ishida, J. Phys.: Conf. Ser. **1052**, 012112 (2018).
23) Y. Wada and R. Hayakawa, J. Appl. Phys. **15**, 2041 (1976).
24) T. Furukawa, M. Date, and E. Fukuda, J. Appl. Phys. **51**, 1135 (1980).
25) O. Pabst, J. Perelaer, E. Beckert, U. S. Schubert, R. Eberhardt, and A. Tunnermann, Org. Electron. **14**, 3423 (2013).
26) T. Kajihara, Y. Ueno, Y. Tsujimura, Y. Koshiba, M. Morimoto, I. Kanno, and K. Ishida, Jpn. J. Appl. Phys. **56**, 04CL04 (2017).
27) M. G. Cepa, K. Engvall, M. Hakkarainen, and A. Kotarba, Prog. Org. Coat. **140**, 105493 (2020).
28) Y. Higashihata, J. Sako, and T. Yagi, Ferroelectrics **32**, 85 (1981).
29) K. Koga, N. Nakano, T. Hattori, and H. Ohigashi, J. Appl. Phys. **67**, 965 (1990).
30) T. Lee, J. Lee, and C. Park, Korean J. Chem. Eng. **19**, 722 (2002).
31) M. J. Herman and M. W. Blair, Polym. Degrad. Stab. **171**, 109024 (2020).
32) K. Tashiro"Crystal structure and phase transition of PVDF and related copolymers," *Ferroelectric Polymer*, ed. H. S. Nalha, (Mercel Dekker, New York, 1995) , p. 63.
33) K. Takashima, K. Ota, M. Yamamoto, M. Takenaka, S. Horie, and K. Ishida, Robomech. J. **6**, 19 (2019).
34) B. Neese, Y. Wang, B. Chu, K. Ren, S. Liu, and Q. M. Zhang, Appl. Phys. Lett. **90**, 242917 (2007).